Sci

Article

Plastic Strain Spread Study for the Optimal Design of Multistep Flexural Steel Beam Elements

Salvatore Benfratello * and **Luigi Palizzolo**

Department of Engineering, Viale delle Scienze, University of Palermo, I-90128 Palermo, Italy; luigi.palizzolo@unipa.it
* Correspondence: salvatore.benfratello@unipa.it

Abstract

The present paper concerns a new formulation of the optimal design problem of I-shaped multistep steel beam elements, based on the study of the plastic strain spread occurring in the relevant elements, with the aim of determining the length involved by the plastic deformation related to assigned load conditions and different constrained beam schemes. Material behavior is assumed as elastic–perfectly plastic, and the hypothesis of plane cross-sections is accepted. The functions defining the plastic strain spread are analytically obtained in the framework of Euler–Bernoulli beam theory. The proposed optimal design problem is a minimum volume one and the new constraint imposed on the length of the plasticized portion ensures that the minimum volume beam element also represents a maximum plastic dissipation one. Furthermore, the solution to the optimal design problem guarantees that the obtained multistep beam element ensures protection against brittle failure of the beam end sections, provides optimal cross-sections of the different portions belonging to Class 1 and ensures a suitable minimum value of the elastic flexural stiffness to respect the constraint on the deflection. Explicit reference is made to the so-called Reduced Beam Section (RBS), which characterizes the described multistep beam elements. Actually, the proposed formulation represents an innovative approach to obtaining an optimal beam element that really satisfies all the resistance, stiffness and ductility behavioral requirements. Some numerical applications conclude the paper, and their results are confirmed by appropriate FEM analyses in ABAQUS environment.

Keywords: steel structures; plastic strains; I-shaped cross-sections; multistep beam elements

Check for updates

Academic Editor: Francesco Tornabene

Received: 4 December 2025
Revised: 4 January 2026
Accepted: 8 January 2026
Published: 12 January 2026

1. Introduction

As it is well known, the current trend in structural construction is to use both traditional and innovative technologies that are aimed at saving energy, comply with circular economy concepts and are environmentally sustainable. Furthermore, concepts of durability with reference to structure lifetime, ease of maintenance, protection against environmental degradation, safety with reference to the different conditions that the structure must satisfy and the behavior that it must ensure under the different intensities and combinations of actions to be withstood during its lifetime, increasingly recommend the use of steel structures. In particular, in the field of civil and industrial engineering, the almost exclusive reference is to three-dimensional steel frames, preferably made using beam elements with standard cross-sections on sale.

There are many requirements that these structures must meet in order to ensure an optimal behavior and they concern both kinematical and mechanical aspects; these requirements are prescribed by the international standards and are suggested in several technical and scientific papers devoted to the solution to analysis for static and/or quasi-static loads, see, e.g., [1–4], seismic load conditions problems, see, e.g., [5–8], design problems, see, e.g., [9], considering both concrete structures, see, e.g., [10], steel structures, see, e.g., [11–14], furtherly considering element slenderness, see, e.g., [15,16], and bracing elements, see, e.g., [17]. They are fundamental constraints for any design problem that may arise.

First of all, it is necessary to satisfy appropriate limit conditions on chosen measures of the displacements and strains such as beam deflection and drifts in serviceability conditions. To satisfy these conditions, a suitable minimum value of the bending stiffness of pillars and beams must be ensured.

At the same time, it is necessary to satisfy appropriate safety conditions involving the generalized stresses which the frame structure suffers in limit collapse conditions. To satisfy these conditions a suitable cross-section geometry must be defined, ensuring sufficient strength capacity.

Furthermore, it must be required that the ductility features of the material and, consequently, of the frame structure are exploited as much as possible. To satisfy this requirement, reference must be made to the beam cross-section resistance; indeed, it is necessary that the beams must be designed as receivers of plastic strains, and so avoiding that the occurring of plastic strains in the pillars can produce local and/or global kinematics.

Finally, taking into account that usually the connection between beams and pillars is constituted by steel plates welded at the beam extremes and bolted to the pillars and that, as known, the welded cross-sections can be subjected to brittle failure, see, e.g., [18–21], it must be required that these cross-sections, usually subjected to the maximum values of the generalized stresses, remain in the elastic regime. It is worth noting that respecting this last condition leaves out the possibility of exploiting the ductility features of the structure, producing, furthermore, a needless structural oversizing.

On the grounds of these remarks, it is clear that the use of beams with constant standard cross-sections, I-shaped or box cross-sections, does not allow the meeting of all the listed requirements in the best possible way.

In the recent past, many studies have been proposed to individuate suitable strategies devoted to reach the better design of steel frame structures respecting the above-listed behavioral requirements. The greater part of these studies concerns the suggestion of technological interventions on the beams of the frame structure with the substantial objective of obtaining both protection of welded extreme cross-sections and exploitation of the ductility features. The suggested technological interventions are suitably supported by numerical and experimental tests. In particular, the principal object of these studies is devoted to the analysis and design of moment resisting steel frames equipped with special devices aimed at improving the frame behavior under static, cyclic and seismic actions. Special attention is devoted to the so-called Reduced Beam Section (RBS) connections.

The first proposed RBS connection, specifically devoted to I-shaped cross-sections, is the dogbone, see, e.g., [22–25], which was experimentally investigated, see, e.g., [26,27], with main application in seismic conditions, see, e.g., [28–32], and in the field of the structural retrofitting, see, e.g., [33]. With the adoption of this technique a suitably chosen portion of the beam is subjected to a geometry reduction consisting of a partial and symmetric cut of the flanges producing the reduction in the strength of the involved beam portion. The main objective of the application of the dogbone technique is to realize specific assigned portions of the beam where the material ductility features can be exploited producing plastic dissipation through the development of plastic hinges. It is worth noting that this technique just partially satisfies the requirements previously listed; indeed, the dogbone technique does not derive from an optimization technique being applied to an initial design which utilizes standard I-shaped cross-sections; furthermore, it does not ensure a complete protection against the brittle failure of the welded end beam cross-section and, obviously, also produces a reduction in the bending stiffness of the involved beam element.

Many other researchers proposed alternative techniques finalized to the same objective, see, e.g., [34–40], investigating numerical, see, e.g., [41–44], and experimental response, see, e.g., [45–47]. Also, the authors of this paper propose a new special device, called Limit Resistance Plastic Device (LRPD), whose main novelty is related to the possibility of ensuring the development of plastic hinges in assigned portions of the involved beams without causing any reduction in the bending stiffness of the beam element, see, e.g., [48–50]. Further papers on LRPD are reported in the literature; they are related to their numerical and experimental behavior, see, e.g., [51,52], as well as to the prevention of brittle failure, see, e.g., [53], and of local buckling, see, e.g., [54], finally extending their application to a plane steel frame, see, e.g., [55].

The most recent version of this device is represented by a short symmetric steel element constituted by three subsequent I-shaped cross-section portions of different, suitably designed geometries. The central portion is the weaker one and it is designed as receiver of plastic strains, while the eternal ones ensure the prefixed bending stiffness of the whole element.

The extension of the basic principle governing the application of the described device to multistep beams, see, e.g., [56,57], is immediate; in other words, instead of operating on an assigned beam and entrusting the device alone with the task of optimally satisfying all the required behavioral requirements, an optimal multistep beam is designed to satisfy all the prescribed requirements, with certain advantages in terms of costs and technology of realization. In its most general form, the multistep beam consists of five subsequent portions and is symmetrical with respect to its mid-span cross-section. The cross-sections of the different portions will generally have different geometries depending on the behavioral requirements, on the acting loads and on the constraint conditions.

Preliminary studies have already been proposed by the authors [58] related to a first formulation of the optimal design of the multistep beams and to the behavioral comparison between the use of RBS device (specifically dogbone) and multistep beam elements. In particular, it is shown that the multistep beam besides possessing the virtuous feature of inducing the occurrence of plastic deformation in prefixed beam portions such as the dogbone, furthermore allows to optimize the beam stiffness independently of the cross-section reduction and ensures the avoiding of the brittle failure in correspondence of the welded cross-sections.

Nevertheless, it must be remarked that, even if the above-referenced preliminary studies showed the full reliability of the multistep beam model, the formulation proposed did not take into account the real plastic strain spread suffered by the sacrificed weak portions of the beam element and, especially, the effective length involved by the plastic strains. It is worth noting that these information results are of central interest for reaching the goal of an optimal beam capable of fully exploiting the material ductility features and avoiding useless wastefulness.

Therefore, this paper proposes an original analytical formulation providing the crucial determination on how the plastic deformation spreads in a bending beam element made of elastic–perfectly plastic material with an I-shaped section, starting from the fully plasticized cross-section. Through this analysis, conducted referring to two different beam schemes (simply supported beam and perfectly clamped beam) subjected to a uniformly distributed load, the length affected by plastic deformation is determined. This length is an essential piece of information for the subsequent design problem and allows also for a correct assessment of the extent of the curvature that develops and of the amount of plastic dissipation that can be generated.

The obtained length and the function trend determined are then used in the formulation of a new optimal design problem aimed at sizing a multistep beam that perfectly complies with all the constraints describing the behavioral requirements mentioned above. The applications are devoted to the case of a perfectly clamped beam subjected to a combination of two different load conditions (serviceability limit load and ultimate limit load) and refer to different approaches as well as different types of cross-sections. The reliability of the obtained results is finally verified by means of suitable 3D FEM elastic plastic analyses performed in ABAQUS® environment. It is worth noting that these results immediately suggest extending the analysis to plane or 3D frames; these applications, together with suitable experimental tests, will be addressed in future studies, which will also explicitly take into account aspects related to the seismic behavior of the structure.

2. Materials and Methods

In the present Section, two fundamental cases are described: the simply supported beam and the perfectly clamped beam, both subjected to a uniformly distributed load. These schemes substantially represent the two typical extreme conditions for beams pertaining to steel frame structures.

2.1. Simply Supported Beam Subjected to a Uniformly Distributed Load

Let us consider a simply supported beam of length ℓ, referred to axes x, y, z, where x is the beam axis and y and z are the central axes of inertia of the relevant cross-section (see Figure 1).

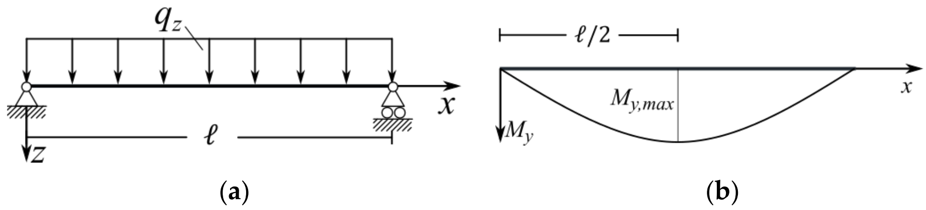

Figure 1. Simply supported beam: (**a**) Structural scheme; (**b**) Bending moment diagram.

Let us assume that the beam cross-section is a constant I-shaped one, symmetric with respect to the y axis, constituted by steel with elastic–perfectly plastic behavior (σ_0 being the yield stress and E Young's modulus) and that it is subjected just to a uniformly distributed load q_z (Figure 1a). The bending moment function shows a parabolic law along the beam axis and reaches its maximum value at the beam midpoint (Figure 1b):

$$M_{y,max} = \frac{q_z \ell^2}{8} \tag{1}$$

Assuming the Bernoulli–Navier hypothesis and indicating with W_{Ey} the elastic resistance modulus of the cross-section, when the maximum bending moment reaches its elastic limit M_{Ey},

$$M_{y,max} = M_{Ey} = W_{Ey}\sigma_0, \tag{2}$$

both the extrados and intrados of the cross-section suffer the yield stress σ_0.

When increasing the acting load, indicated with W_{py}, the plastic resistance modulus of the cross-section, when the maximum bending moment reaches its yield value M_{py},

$$M_{y,max} = M_{py} = W_{py}\sigma_0, \tag{3}$$

the whole cross-section suffers plastic deformations and a plastic hinge arises with the bending curvature tending towards infinity.

We want to calculate the length of the portion where the plastic strains occur (suitable neighborhood of the beam midpoint) when $M_{y,max} = M_{py}$, together with the trend of the plasticization profile in this range. Therefore, let us impose the following:

$$M_{y,max} = M_y\left(\frac{\ell}{2}\right) = M_{py} = \frac{q_{z,p}\ell^2}{8} \tag{4}$$

where

$$q_{z,p} = \frac{8M_{py}}{\ell^2} \tag{5}$$

is the limit load value which causes the plasticization of the whole cross-section at the beam midpoint.

The bending moment law in condition of impending whole plasticization of the midpoint beam cross-section holds:

$$M_y(x) = \frac{q_{z,p}\ell}{2}x - \frac{q_{z,p}x^2}{2} = 4M_{py}\frac{x}{\ell} - 4M_{py}\frac{x^2}{\ell^2} = 4M_{py}\frac{x}{\ell^2}(\ell - x) \tag{6}$$

Let $x_E < \ell/2$ be the abscissa where the bending moment reaches its elastic limit value M_{Ey}. It results as follows:

$$M_y(x_E) = M_{Ey} = 4M_{py}\frac{x_E}{\ell^2}(\ell - x_E) \tag{7}$$

which can be written in two alternative ways as follows:

$$W_{Ey}\sigma_0 = 4W_{py}\sigma_0\frac{x_E}{\ell^2}(\ell - x_E) \tag{8a}$$

$$4W_{py}\frac{x_E^2}{\ell^2} - 4W_{py}\frac{x_E}{\ell} + W_{Ey} = 0 \tag{8b}$$

from which it can be deduced that

$$x_E^2 - \ell x_E + \frac{W_{Ey}}{W_{py}}\frac{\ell^2}{4} = 0 \tag{9}$$

and, consequently,

$$x_E = \frac{\ell}{2} \pm \sqrt{\left(\frac{\ell}{2}\right)^2 - \left(\frac{\ell}{2}\right)^2\frac{W_{Ey}}{W_{py}}} = \frac{\ell}{2} \pm \frac{\ell}{2}\sqrt{1 - \frac{W_{Ey}}{W_{py}}} = \frac{\ell}{2}\left(1 \pm \sqrt{1 - \frac{W_{Ey}}{W_{py}}}\right) \tag{10}$$

Obviously, x_E must not be greater than $\frac{\ell}{2}$ and, therefore, the solution reads

$$x_E = \frac{\ell}{2}\left(1 - \sqrt{1 - \frac{W_{Ey}}{W_{py}}}\right) \tag{11}$$

The length of the beam portion where plastic strains arise is

$$\ell_p = 2\left(\frac{\ell}{2} - x_E\right) = \ell\sqrt{1 - \frac{W_{Ey}}{W_{py}}} = \ell\sqrt{\frac{W_{py} - W_{Ey}}{W_{py}}} \tag{12}$$

and it just depends on the beam cross-section geometry.

The form of the plastic resistance modulus W_{py} and that of the elastic resistance modulus W_{Ey} are reported in the following. In both cases the inner arc radius connecting flanges with web is disregarded. Such a position is widely justified because in the present study beams constituted by I-shaped cross-sections made in the factory are considered and because, from an engineering perspective, the influence of these connections is usually negligible.

The plastic resistance modulus can be written in the following alternative forms:

$$W_{py} = bt_f\left(h - t_f\right) + t_w\left(\frac{h}{2} - t_f\right)^2 = \frac{bh^2}{2} - \frac{(b - t_w)\left(h - 2t_f\right)^2}{4} \tag{13}$$

where the utilized symbols defining the cross-section geometry are reported in the following Figure 2.

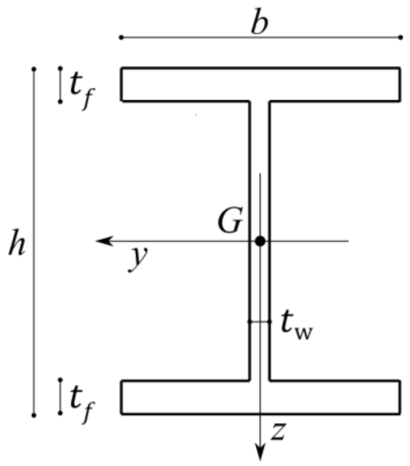

Figure 2. Geometrical characteristics of the I cross-section.

In order to define the form of the elastic resistance modulus, reference can be made to the form of the limit elastic bending moment M_{Ey}:

$$M_{Ey} = \left[\sigma_0 b + \frac{2\sigma_0}{h}\left(\frac{h}{2} - t_f\right)b\right]\frac{t_f}{2}(h - 2d_G) + \frac{2\sigma_0}{h}\left(\frac{h}{2} - t_f\right)^2\frac{t_w}{2}\frac{2}{3}\left(h - 2t_f\right) \tag{14}$$

where the first addendum is related to the contribution of the flanges (F_f) and the second one to that of the web (F_w) (see Figure 3). In particular, in the first addendum, d_G represents the distance (measured along z) from the intrados (or extrados) of the barycenter of the stress volume related to the flange; with reference to the symbols of Figure 3b, it results in the following:

$$d_G = \frac{c(2b_1 + b_2)}{3(b_1 + b_2)} \tag{15}$$

Therefore, utilizing appropriate symbols (Figure 2) gives

$$d_G = \frac{t_f\left[\frac{4}{h}\left(\frac{h}{2} - t_f\right) + 1\right]}{3\left[\frac{2}{h}\left(\frac{h}{2} - t_f\right) + 1\right]} = \frac{t_f\left(3h - 4t_f\right)}{6\left(h - t_f\right)} \tag{16}$$

Therefore, it is possible to derive

$$W_{Ey} = \frac{M_{Ey}}{\sigma_0} = \left[b + \frac{2}{h}\left(\frac{h}{2} - t_f\right)b\right]\frac{t_f}{2}(h - 2d_G) + \frac{2}{h}\left(\frac{h}{2} - t_f\right)^2\frac{t_w}{2}\frac{2}{3}\left(h - 2t_f\right) \tag{17}$$

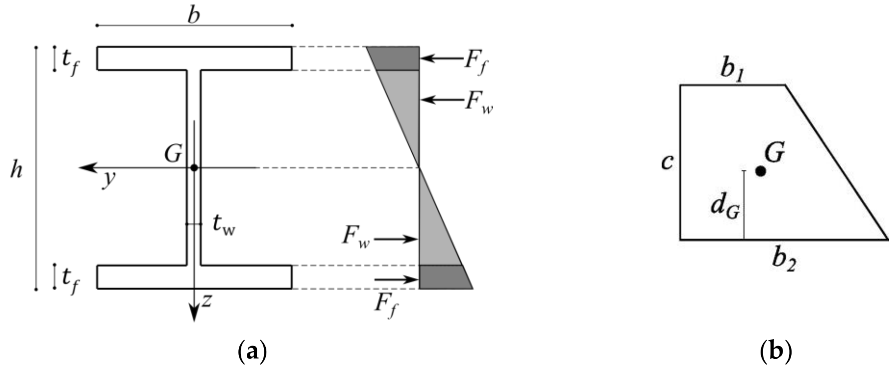

Figure 3. Determination of the elastic resistance modulus: (**a**) Reference stress diagram; (**b**) Geometrical scheme for the determination of the barycenter of the stress volume related to the flange.

With simple mathematics, this provides

$$\begin{aligned} W_{Ey} &= \tfrac{t_f b}{h}\left(h - t_f\right)(h - 2d_G) + \tfrac{4}{3}\tfrac{t_w}{h}\left(\tfrac{h}{2} - t_f\right)^3 j \\ &= \tfrac{t_f b}{h}\left(h^2 - 2t_f h + \tfrac{4}{3}t_f^2\right) + \tfrac{4}{3}\tfrac{t_w}{h}\left(\tfrac{h}{2} - t_f\right)^3 \end{aligned} \quad (18)$$

Alternatively, it is possible to determine W_{Ey} by the moment of inertia I_y of the cross-section:

$$I_y = \frac{bh^3}{12} - \frac{(b - t_w)\left(h - 2t_f\right)^3}{12} \quad (19)$$

from which the following form can be deduced:

$$W_{Ey} = \frac{2I_y}{h} = \frac{bh^2}{6} - \frac{(b - t_w)\left(h - 2t_f\right)^3}{6h} \quad (20)$$

which, with easy mathematics, provides the same form as in Equation (18).

In the beam portion between x_E and $\frac{\ell}{2}$, i.e., in the range $0 \le \xi \le \frac{\ell}{2}\sqrt{\frac{W_{py} - W_{Ey}}{W_{py}}}$, the bending moment parabolically increases from M_{Ey} to M_{py} and in this range the cross-sections (except for the range extremes) are partially plasticized (see Figure 4).

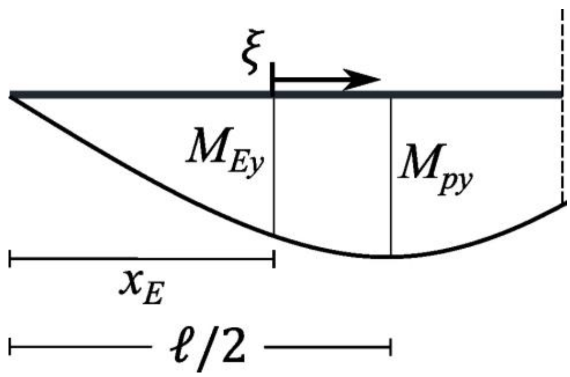

Figure 4. Local reference system adopted in the first half portion of the beam affected by plastic strains for the determination of function $z_p(\xi)$.

In the defined range the bending moment function can be written in the form

$$
\begin{aligned}
M_y(\xi) = M_{Ey} + \left(\tfrac{q_{z,p}\ell}{2} - q_{z,p}x_E\right)\xi - \tfrac{q_{z,p}\xi^2}{2} &= M_{Ey} + q_{z,p}\left(\tfrac{\ell}{2} - x_E\right)\xi - \tfrac{q_{z,p}\xi^2}{2} \\
&= M_{Ey} + \tfrac{8M_{py}}{\ell^2}\left(\tfrac{\ell}{2} - x_E\right)\xi - \tfrac{4M_{py}\xi^2}{\ell^2} \\
&= M_{Ey} + \tfrac{4M_{py}}{\ell^2}\left[(\ell - 2x_E)\xi - \xi^2\right] \\
&= M_{Ey} + \tfrac{4M_{py}}{\ell^2}\xi[\ell - 2x_E - \xi]
\end{aligned}
\tag{21}
$$

from which the "elastic plastic resistance modulus function" can be deduced:

$$
W_y(\xi) = \frac{M_y(\xi)}{\sigma_0} = W_{Ey} + \frac{4W_{py}}{\ell^2}\xi[\ell - 2x_E - \xi] \tag{22}
$$

First of all, we want to treat the case when just the flanges (although just partially) suffer plastic strains, i.e., for $\frac{h}{2} - t_f \leq z_p \leq \frac{h}{2}$, z_p being the minimum distance between the plasticized fibers and the y barycentric axis (see Figure 5).

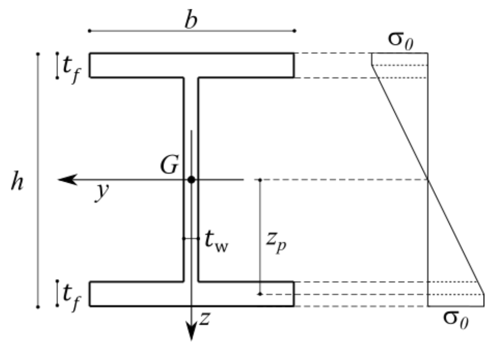

Figure 5. Typical stress distribution when the flanges are partially plasticized.

In this case the acting bending moment has the form

$$
\begin{aligned}
M_y(z_p) = \sigma_0 b\left(\tfrac{h}{2} - z_p\right)\left(\tfrac{h}{2} + z_p\right) &+ b\left[\sigma_0 + \tfrac{\sigma_0}{z_p}\left(\tfrac{h}{2} - t_f\right)\right]\left(t_f - \tfrac{h}{2} + z_p\right)(z_p - d_G^*) \\
&+ \tfrac{\sigma_0}{z_p}\left(\tfrac{h}{2} - t_f\right)^2 \tfrac{t_w}{2}\tfrac{2}{3}\left(h - 2t_f\right)
\end{aligned}
\tag{23}
$$

with

$$
d_G^* = \frac{\left(t_f - \frac{h}{2} + z_p\right)\left[\frac{2}{z_p}\left(\frac{h}{2} - t_f\right) + 1\right]}{3\left[\frac{1}{z_p}\left(\frac{h}{2} - t_f\right) + 1\right]} = \frac{\left(t_f - \frac{h}{2} + z_p\right)\left(h - 2t_f + z_p\right)}{3\left[\frac{h}{2} - t_f + z_p\right]} \tag{24}
$$

from which it is possible to deduce

$$
\begin{aligned}
W_y(z_p) = b\left(\tfrac{h}{2} - z_p\right)\left(\tfrac{h}{2} + z_p\right) &+ b\left[1 + \tfrac{1}{z_p}\left(\tfrac{h}{2} - t_f\right)\right]\left(t_f - \tfrac{h}{2} + z_p\right)(z_p - d_G^*) \\
&+ \tfrac{1}{z_p}\left(\tfrac{h}{2} - t_f\right)^2 \tfrac{t_w}{2}\tfrac{2}{3}\left(h - 2t_f\right)
\end{aligned}
\tag{25}
$$

which, with simple mathematics, provides:

$$
W_y(z_p) = b\left(\frac{h^2}{4} - z_p^2\right) + \frac{b}{z_p}\left[z_p^2 - \left(\frac{h}{2} - t_f\right)^2\right](z_p - d_G^*) + \frac{2t_w}{3z_p}\left(\frac{h}{2} - t_f\right)^3 \tag{26}
$$

By utilizing this last equation and Equation (22) and setting

$$
z_p = \frac{h}{2} - t_f, \tag{27}
$$

the value $\xi = \xi_e$, which defines the position of the cross-section in which just the whole flanges are plasticized, is determined, and, consequently, always utilizing Equations (22) and (26), it is possible to obtain the trend of the function $z_p(\xi)$ in the range $0 \leq \xi \leq \xi_e$.

Now, we want to define the form of $W_y(z_p)$ when the web also (although just partially) suffers plastic strains, i.e., for $0 \leq z_p \leq \frac{h}{2} - t_f$ (see Figure 6).

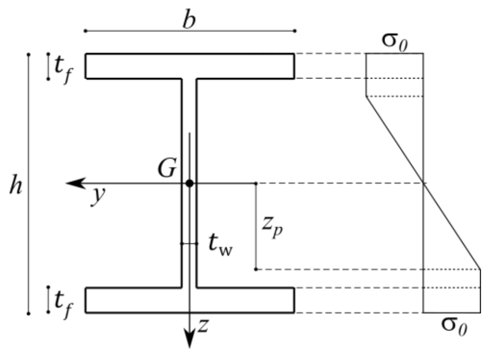

Figure 6. Typical stress distribution when the web is partially plasticized.

In this case the acting bending moment has the form

$$M_y(z_p) = \sigma_0 b t_f \left(h - t_f\right) + \sigma_0 t_w \left(\frac{h}{2} - t_f - z_p\right)\left(\frac{h}{2} - t_f + z_p\right) + \sigma_0 \frac{t_w z_p}{2} \frac{4}{3} z_p \tag{28}$$

from which it is possible to deduce

$$W_y(z_p) = b t_f \left(h - t_f\right) + t_w \left[\left(\frac{h}{2} - t_f\right)^2 - z_p^2\right] + \frac{2}{3} t_w z_p^2 \tag{29}$$

Finally, the trend of the function $z_p(\xi)$ can be deduced by identifying this last equation with Equation (22) in the range $\xi_e \leq \xi \leq \frac{\ell}{2}\sqrt{\frac{W_{py} - W_{Ey}}{W_{py}}}$.

In Figure 7a,b the function $z_p(\xi)$ has been reported in the domain $(0, x_E)$ for two typical standard steel profiles on sale: HEA300 and IPE300.

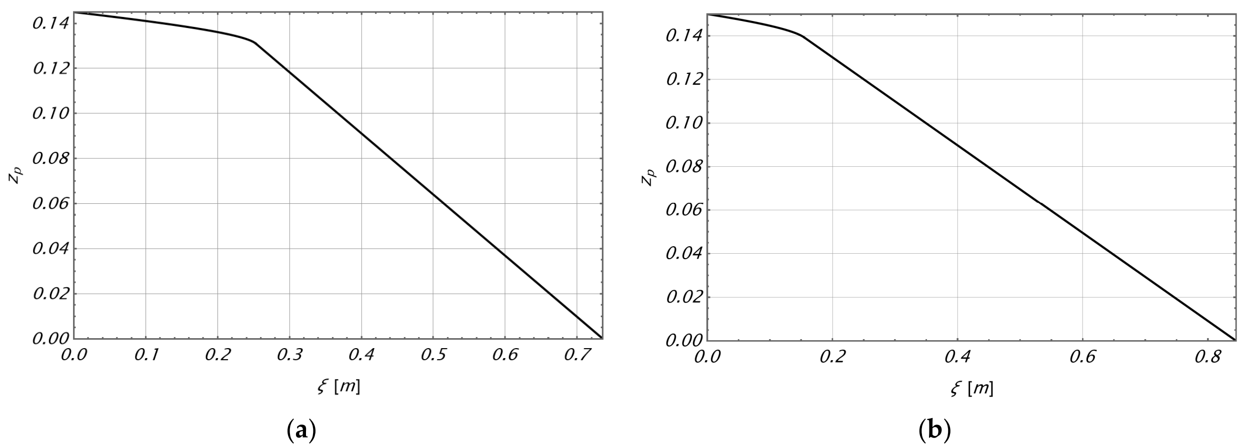

Figure 7. Evolution of z_p for simply supported beam: (**a**) Case of HEA 300 cross-section; (**b**) Case of IPE 300 cross-section.

The ratio between ξ_e and x_E depends on the different cross-section geometry, while the consistent length of the beam portion where the plastic strains occur depends on the moderate slope of the bending moment diagram. Furthermore, in Table 1, the obtained results for both the studied profiles are synthesized.

Table 1. Results for the simply supported beam.

Description	HEA 300	IPE 300
Length ℓ	5.0 m	5.0 m
Base b	300 mm	150 mm
Height h	290 mm	300 mm
Web thickness t_w	8.5 mm	7.1 mm
Flange thickness t_f	14.0 mm	10.7 mm
x_e	1.764 m	1.655 m
ℓ_p	1.472 m	1.691 m
ξ_e	0.253 m	0.155 m

Now, we want to determine the trend of the curvature function.

The limit elastic curvature k_{Ey} in correspondence to the cross-section of abscissa x_E holds:

$$k_{Ey} = \frac{M_{Ey}}{EI_y} \tag{30}$$

In the range $0 \leq \xi \leq \frac{\ell}{2}\sqrt{\frac{W_{py}-W_{Ey}}{W_{py}}}$ (starting from the cross-section of abscissa x_E) the total curvature,

$$k_y = k_{Ey} + k_{py}, \tag{31}$$

is given as the sum of the elastic curvature k_{Ey} and of the plastic curvature k_{py}.

In the first portion of this range, i.e., for $0 \leq \xi \leq \xi_e$ the total curvature shows the following form:

$$k_{y,1}(\xi) = \frac{\sigma_0}{Ez_p(\xi)} \tag{32}$$

with function $z_p(\xi)$ above determined by utilizing Equations (22) and (26):

$$\begin{aligned} W_{Ey} + \tfrac{4W_{py}}{\ell^2}\xi[\ell - 2x_E - \xi] \\ = b\tfrac{h^2}{4} - bz_p d_G^* - b\left(\tfrac{h}{2} - t_f\right)^2 + \tfrac{b}{z_p}\left(\tfrac{h}{2} - t_f\right)^2 d_G^* + \tfrac{2t_w}{3z_p}\left(\tfrac{h}{2} - t_f\right)^3 \end{aligned} \tag{33}$$

In the second portion of the above-defined range, i.e., for $\xi_e \leq \xi \leq \frac{\ell}{2}\sqrt{\frac{W_{py}-W_{Ey}}{W_{py}}}$, the total curvature shows the following analogous form:

$$k_{y,2}(\xi) = \frac{\sigma_0}{Ez_p(\xi)} \tag{34}$$

but with the function $z_p(\xi)$ above determined by utilizing Equations (22) and (29):

$$W_{Ey} + \frac{4W_{py}}{\ell^2}\xi[\ell - 2x_E - \xi] = bt_f\left(h - t_f\right) + t_w\left[\left(\frac{h}{2} - t_f\right)^2 - z_p^2\right] + \frac{2}{3}t_w z_p^2 \tag{35}$$

The relative rotation between the cross-section of abscissa x_E and the midpoint beam cross-section holds:

$$\xi_{\varphi,1\_2} = \int_0^{\xi_e} k_{y,1}(\xi)d\xi + \int_{\xi_e}^{\frac{\ell}{2}\sqrt{\frac{W_{py}-W_{Ey}}{W_{py}}}} k_{y,2}(\xi)d\xi \tag{36}$$

The total dissipation,

$$D_{1\_2} = D_{E,1\_2} + D_{p,1\_2}, \tag{37}$$

sum of the elastic and the plastic one in the two subsequent portions of the range $0 \leq \xi \leq \ell\sqrt{\frac{W_{py}-W_{Ey}}{W_{py}}}$, holds:

$$D_{1\_2} = 2\int_0^{\xi_e} M_y(\xi)\left[k_{y,1}(\xi)\right]d\xi + 2\int_{\xi_e}^{\frac{\ell}{2}\sqrt{\frac{W_{py}-W_{Ey}}{W_{py}}}} M_y(\xi)\left[k_{y,2}(\xi)\right]d\xi \tag{38}$$

while the only plastic dissipation in the same range holds:

$$D_{p,1\_2} = 2\int_0^{\xi_e} M_y(\xi)\left[k_{y,1}(\xi) - k_{Ey}\right]d\xi + 2\int_{\xi_e}^{\frac{\ell}{2}\sqrt{\frac{W_{py}-W_{Ey}}{W_{py}}}} M_y(\xi)\left[k_{y,2}(\xi) - k_{Ey}\right]d\xi \tag{39}$$

2.2. Perfectly Clamped Beam Subjected to a Uniformly Distributed Load

Let us consider yet the same beam of length ℓ as described above but perfectly clamped at its extremes and yet subjected to a uniformly distributed load q_z (Figure 8a).

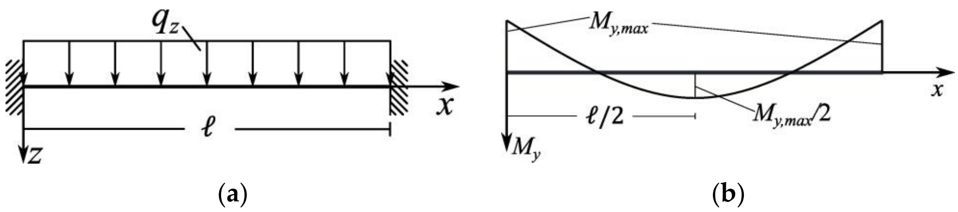

Figure 8. Perfectly clamped beam: (**a**) Structural scheme; (**b**) Bending moment diagram.

The bending moment function shows a parabolic law along the beam axis and reaches its maximum value simultaneously at the clamped cross-sections (Figure 8b):

$$M_{y,max} = |M_y(0)| = |M_y(\ell)| = \frac{q_z\ell^2}{12} \tag{40}$$

Assuming the same hypotheses as above and following the same approach, we want to calculate the length of the portion where the plastic strains occur (starting from the clamped cross-sections) when $M_{y,max} = M_{py}$, together with the trend of the plasticization profile in this range.

Therefore, let us impose the following:

$$M_{y,max} = |M_y(0)| = M_{py} = \frac{q_{z,p}\ell^2}{12} \tag{41}$$

where

$$q_{z,p} = \frac{12M_{py}}{\ell^2} \tag{42}$$

is the limit load value which causes the plasticization of the whole cross-section at the extremes of the beam $(x = 0 \text{ and } x = \ell)$.

The bending moment law in condition of impending whole plasticization of the relevant beam cross-sections holds:

$$\begin{aligned} M_y(x) &= -M_{py} + \tfrac{q_{z,p}\ell}{2}x - \tfrac{q_{z,p}x^2}{2} = -M_{py} + \tfrac{6M_{py}}{\ell}x - \tfrac{6M_{py}x^2}{\ell^2} = M_{py}\left(\tfrac{6x}{\ell} - \tfrac{6x^2}{\ell^2} - 1\right) \\ &= M_{py}\left[6x\tfrac{(\ell-x)}{\ell^2} - 1\right] \end{aligned} \tag{43}$$

Starting from the initial cross-section, let $x_E < \frac{\ell}{2}$ be the abscissa where the bending moment reaches its elastic limit value $-M_{Ey}$ (Figure 9).

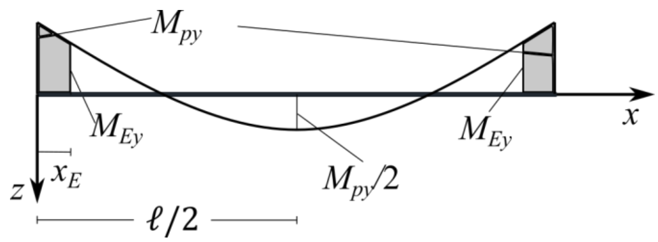

Figure 9. Portions of the beam affected by plastic strains.

The elastic limit bending moment value is given by

$$M_y(x_E) = -M_{Ey} = M_{py}\left[6x_E\frac{(\ell - x_E)}{\ell^2} - 1\right] \tag{44}$$

which can be written in the following alternative ways:

$$-W_{Ey}\sigma_0 = W_{py}\sigma_0\left[6x_E\frac{(\ell - x_E)}{\ell^2} - 1\right] \tag{45a}$$

$$6W_{py}\frac{x_E^2}{\ell^2} - 6W_{py}\frac{x_E}{\ell} + W_{py} - W_{Ey} = 0 \tag{45b}$$

from which it can be deduced that

$$x_E^2 - x_E\ell + \frac{W_{py} - W_{Ey}}{6W_{py}}\ell^2 = x_E^2 - x_E\ell + \frac{2}{3}\frac{W_{py} - W_{Ey}}{W_{py}}\left(\frac{\ell}{2}\right)^2 = 0, \tag{46}$$

i.e.,

$$\begin{aligned} x_E &= \frac{\ell}{2} \pm \sqrt{\left(\frac{\ell}{2}\right)^2 - \left(\frac{\ell}{2}\right)^2 \frac{2}{3}\frac{W_{py}-W_{Ey}}{W_{py}}} = \frac{\ell}{2} \pm \frac{\ell}{2}\sqrt{1 - \frac{2}{3}\frac{W_{py}-W_{Ey}}{W_{py}}} \\ &= \frac{\ell}{2}\left(1 \pm \sqrt{1 - \frac{2}{3}\frac{W_{py}-W_{Ey}}{W_{py}}}\right) \end{aligned} \tag{47}$$

Obviously, x_E must not be greater than $\frac{\ell}{2}$ and, therefore, the solution reads

$$x_E = \frac{\ell}{2}\left(1 - \sqrt{1 - \frac{2}{3}\frac{W_{py} - W_{Ey}}{W_{py}}}\right) = \frac{\ell}{2}\left(1 - \sqrt{\frac{W_{py} + 2W_{Ey}}{3W_{py}}}\right) \tag{48}$$

and this value defines the length of the beam portion where plastic strains arise:

$$\ell_p \equiv x_E \tag{49}$$

In the range between 0 and x_E $\left[0 \le \xi \le \frac{\ell}{2}\left(1 - \sqrt{\frac{W_{py}+2W_{Ey}}{3W_{py}}}\right)\right]$, the bending moment parabolically increases from $-M_{py}$ to $-M_{Ey}$ and in this range the cross-sections (except for the range extremes) are partially plasticized (Figure 10).

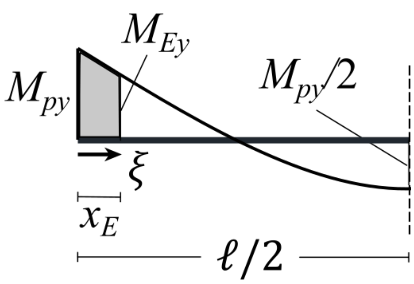

Figure 10. Local reference system adopted in the beam affected by plastic strains for the determination of function $z_p(\xi)$.

The bending moment function has the form

$$M_y(\xi) = M_{py}\left[6\xi\frac{(\ell-\xi)}{\ell^2} - 1\right] \tag{50}$$

from which the "elastic plastic resistance modulus function" can be deduced:

$$W_y(\xi) = \frac{|M_y(\xi)|}{\sigma_0} = W_{py}\left[1 - 6\xi\frac{(\ell-\xi)}{\ell^2}\right] \tag{51}$$

First of all, we want to treat the case when $0 \le z_p \le \frac{h}{2} - t_f$, with z_p always defining the minimum distance between the plasticized fibers and the y barycentric axis (see previous Figure 6). By utilizing Equations (29) and (51) and imposing

$$z_p = \frac{h}{2} - t_f \tag{52}$$

the value $\xi = \xi_e$ where just the flanges are plasticized is found and, as a consequence, in the range $0 \le \xi \le \xi_e$ the function $z_p(\xi)$ is determined.

Referring now to the case when $\frac{h}{2} - t_f \le z_p \le \frac{h}{2}$, i.e., in the range $\xi_e \le \xi \le \frac{\ell}{2}\left(1 - \sqrt{\frac{W_{py}+2W_{Ey}}{3W_{py}}}\right)$ (see previous Figure 5), the function $z_p(\xi)$ is determined by utilizing Equations (26) and (51).

In Figure 11a,b the function $z_p(\xi)$ has been reported in the domain $(0, x_E)$ for two typical standard steel profiles on sale: HEA300 and IPE300.

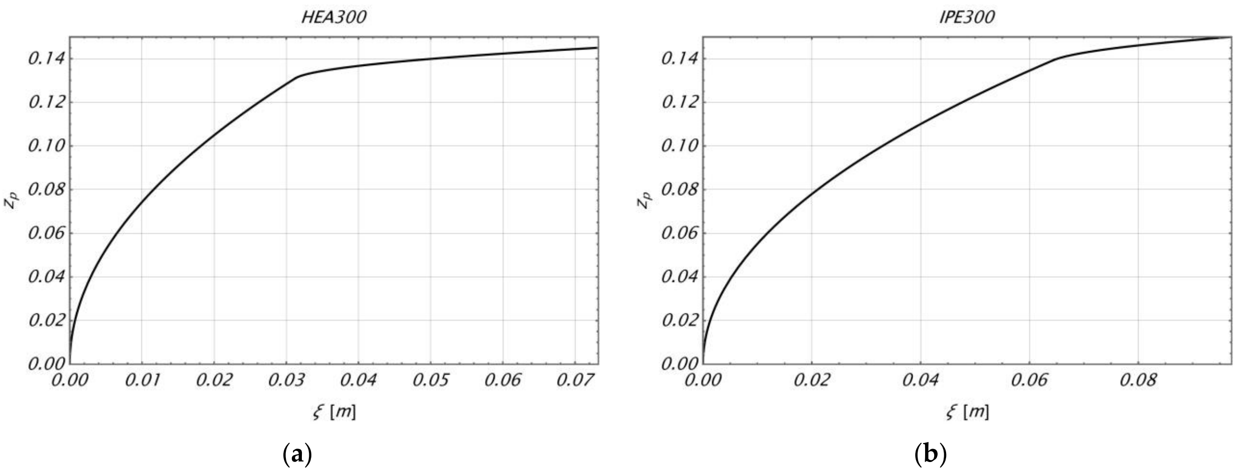

Figure 11. Evolution of z_p for perfectly clamped beam: (**a**) Case of HEA 300 cross-section; (**b**) Case of IPE 300 cross-section.

As previously stated, the ratio between ξ_e and x_E depends on the different cross-section geometry, while the very short length of the beam portion where the plastic strains occur depends on the great slope of the bending moment diagram. In Table 2 the obtained results for both the studied profiles are synthesized.

With the same procedure as before, in both the ranges where plastic strains occur the total curvature can be determined as function of $z_p(\xi)$.

The plastic dissipation in the entire beam holds:

$$D_{p,1\_2} = 2\left\{\int_0^{\xi_e} M_y(\xi)\left[k_{y,1}(\xi) - k_{Ey}\right]d\xi + \int_{\xi_e}^{\frac{\ell}{2}\left(1-\sqrt{\frac{W_{py}+2W_{Ey}}{3W_{py}}}\right)} M_y(\xi)\left[k_{y,2}(\xi) - k_{Ey}\right]d\xi\right\} \tag{53}$$

where $k_{y,1}(\xi)$ is the total curvature occurring in the range $0 \leq \xi \leq \xi_e$ and $k_{y,2}(\xi)$ is the total curvature occurring in the range $\xi_e \leq \xi \leq \frac{\ell}{2}\left(1 - \sqrt{\frac{W_{py}+2W_{Ey}}{3W_{py}}}\right)$, while the bending moment function $M_y(\xi)$ is given by Equation (50).

Table 2. Results for the perfectly clamped beam.

Description	HEA 300	IPE 300
Length ℓ	5.0 m	5.0 m
Base b	300 mm	150 mm
Height h	290 mm	300 mm
Web thickness t_w	8.5 mm	7.1 mm
Flange thickness t_f	14.0 mm	10.7 mm
x_e	0.073 m	0.097 m
ℓ_p	0.073 m	0.097 m
ξ_e	0.031 m	0.064 m

3. Optimal Design of Multistep Beams

In steel frame structures, the beams are usually subjected to uniformly distributed loads and constrained to the pillars by connections that can be modeled as simple hinges or as moment resisting ones, showing a limit behavior as described about.

Actually, the model that better describes the real behavior is that of the perfectly clamped beam; indeed, the connection realized is usually a moment-resisting one and the maximum bending moments always occur at the beam extremes.

Referring to this last model, we want to examine the requisites which optimize the behavior of the typical beam.

As known and previously described in the Introduction, both limit conditions on displacements and strains in serviceability conditions and safety conditions expressed in terms of generalized stresses in limit collapse conditions must be satisfied. Furthermore, the material ductility features must be suitably exploited, appropriately designing the beams as receivers of plastic strains. Finally, the possible brittle failure must be avoided in all the portions which undergo welding processes.

In order to optimally reach all these goals, multistep I-shaped beam elements can be usefully designed as described below.

For the sake of simplicity, let us consider the case of a perfectly clamped beam of length ℓ, subjected to a uniformly distributed load q_z.

With the aim of designing a beam which possesses all the above-mentioned features, reference must be made to a multistep beam constituted by five subsequent portions, each characterized by a constant I-shaped cross-section with suitable geometry (see Figure 12).

The beam is characterized by symmetry with respect to its midspan section. In particular, the two more external portions of the multistep beam must ensure that the elastic limit is not exceeded, avoiding any possible risk of brittle failure; the two subsequent portions must ensure the maximum (optimum) exploitation of the ductility features of the material and the central portion must ensure suitable bending stiffness of the whole beam in order to respect the constraints on the displacements and/or strains.

Consequently, the two external portions will have a cross-section greater than the two subsequent ones, while the central portion cross-section geometry will depend on the geometry of the other described portions.

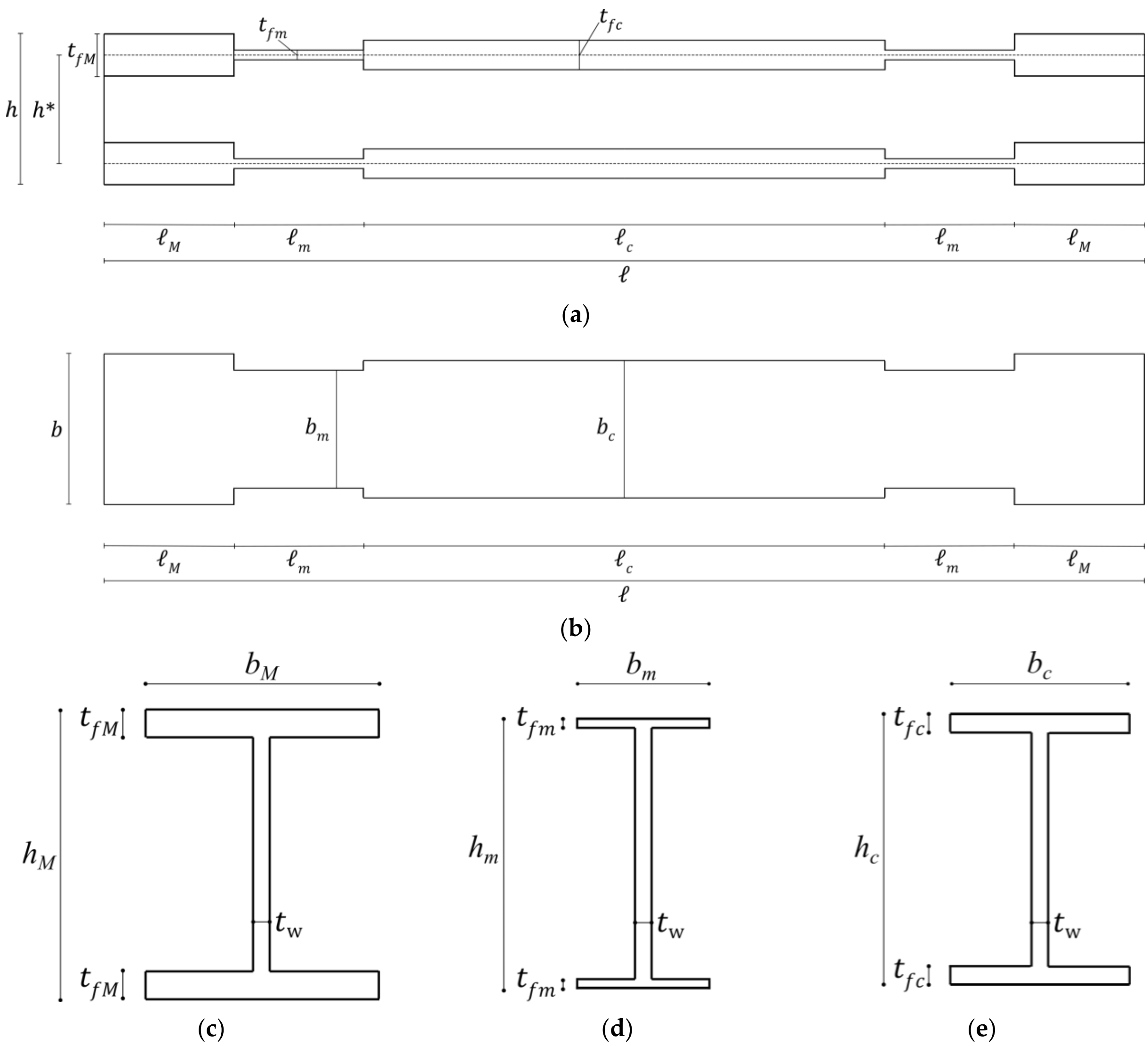

Figure 12. Multistep beam geometry: (**a**) Lateral view; (**b**) Upper view; (**c**) Cross-section of the external strong "*M*" portions; (**d**) Cross-section of the weak "*m*" portions; (**e**) Cross-section of the central "*c*" portion.

To formulate the optimal design problem (minimum volume), considering that we want to utilize I-shaped cross-sections, the measures of the rectangle (base b and height h) realizing the contour of the greater cross-section are assigned as well as the thickness of the web t_w, assumed equal for all the portions. Furthermore, we assume that the flanges of all the portions have a common medium plane, so as it is possible to define the measure h^* as the distance between the medium planes of the relevant flanges.

The data of the optimal design problem are b, h and t_w, while the design variables are t_{fM}, t_{fm}, t_{fc}, b_m, b_c, ℓ_M, referring to the symbols reported in Figure 12, assuming $b_M = b$ and $h_M = h$.

Other relevant quantities, functions of the design variables, are

$$h^* = h - t_{fM} \tag{54}$$

$$A_i = 2b_i t_{fi} + t_w \left(h^* - t_{fi} \right) \ \ (i = M, m, c) \tag{55}$$

$$W_{Eyi} = \frac{t_{fi}b_i}{h^*+t_{fi}}\left[\left(h^*+t_{fi}\right)^2 - 2t_{fi}\left(h^*+t_{fi}\right) + \frac{4}{3}t_{fi}^2\right] + \frac{4}{3}\frac{t_w}{h^*+t_{fi}}\left[\frac{h^*+t_{fi}}{2} - t_{fi}\right]^3 \quad (i = M, m, c) \tag{56}$$

$$W_{pyi} = \frac{b_i\left(h^*+t_{fi}\right)^2}{4} - \frac{(b_i - t_w)\left(h^*-t_{fi}\right)^2}{4} \quad (i = M, m, c) \tag{57}$$

$$\ell_m = \frac{\ell}{2}\left(1 - \sqrt{\frac{W_{py}+2W_{Ey}}{3W_{py}}}\right) \tag{58}$$

$$\ell_c = \ell\sqrt{\frac{W_{py}+2W_{Ey}}{3W_{py}}} - 2\ell_M \tag{59}$$

$$I_i = 2\frac{1}{12}b_i t_{fi}^3 + 2b_i t_{fi}\left(\frac{h^*}{2}\right)^2 + \frac{t_w\left(h^*-t_{fi}\right)^2}{12} \quad (i = M, m, c) \tag{60}$$

where A_i $(i = M, m, c)$ are the measures of the cross-section areas of the different beam portions; W_{Eyi} $(i = M, m, c)$ and W_{pyi} $(i = M, m, c)$ are the elastic and plastic resistance moduli of the cross-sections of the different beam portions; ℓ_m is the length of the portion with lesser strength strictly sufficient to guarantee full plasticization of the cross-section that suffers the greater generalized stress and to ensure the maximum possible plastic dissipation; ℓ_c is the length of the central portion; and I_i $(i = M, m, c)$ are the area moments of inertia of the cross-sections of the different beam portions. In the foregoing sentences the subscript M refers to the external strong portions, the subscript m refers to the weak portions and the subscript c refers to the central portion.

On the ground of the results obtained in the previous section and with reference to the symbols reported in Figure 12, the minimum volume search problem can be formulated as follows:

$$\min_{(t_{fM},t_{fm},t_{fc},b_m,b_c,\ell_M)} V = \min_{(t_{fM},t_{fm},t_{fc},b_m,b_c,\ell_M)} 2(\ell_M A_M + \ell_m A_m) + \ell_c A_c \tag{61a}$$

subjected to

$$\frac{b_M - 3t_w}{18}\sqrt{\frac{\sigma_0}{235}} \leq t_{fM} \leq \frac{h}{2} \tag{61b}$$

$$\frac{b_m - 3t_w}{18}\sqrt{\frac{\sigma_0}{235}} \leq t_{fm} \leq t_{fM} \tag{61c}$$

$$\frac{b_c - 3t_w}{18}\sqrt{\frac{\sigma_0}{235}} \leq t_{fc} \leq \frac{h}{2} \tag{61d}$$

$$3t_w \leq b_m \leq b \tag{61e}$$

$$b_m \leq b_c \leq b \tag{61f}$$

$$\ell_m \leq \ell_M \leq \frac{\ell}{2} \tag{61g}$$

$$\frac{\xi_S q_z}{384\ E}\left[\frac{16\ \ell_M{}^3(\ell_c+2\ell_m+\ell_M)}{I_M} + \frac{16\ \ell_m\left(\ell_m{}^2(\ell_c+\ell_m)+\ell_m(3\ \ell_c+4\ell_m)\ell_M+3(\ell_c+2\ \ell_m)\ell_M{}^2+2\ \ell_M{}^3\right)}{I_m} + \frac{\ell_c\left(\ell_c{}^3+8\ell_c{}^2(\ell_m+\ell_M)+24\ \ell_c(\ell_m+\ell_M)^2+16(\ell_m+\ell_M)^3\right)}{I_c}\right] \leq f_{adm} \tag{61h}$$

$$W_{EyM} \geq W_{pym} + \frac{\eta_0 \xi_L q_z}{2\ \sigma_0}\ell_M(\ell - \ell_M) \tag{61i}$$

$$W_{pym} = \frac{\eta_0 \xi_L q_z}{2\sigma_0}\left[\frac{\ell^2}{6} - \ell \cdot \ell_M + \ell_M^2\right] \tag{61j}$$

$$W_{Eym} \le W_{Eyc} \tag{61k}$$

$$W_{Eyc} \ge \frac{\eta_0 \xi_L}{\sigma_0}\frac{q_z}{8}(\ell - 2\ell_M - 2\ell_m)^2 - \eta_0 W_{Eym} \tag{61l}$$

In the above-formulated problem, ξ_S is an appropriate load multiplier related to the serviceability conditions, ξ_L is an appropriate load multiplier related to limit collapse conditions and η_0 is a material safety factor suitably introduced. Equations (61b–g) represent the constraints on the design variables. In particular, Equations (61b–d) are geometrical and mechanical constraints; indeed, they impose that all the cross-sections belong to Class 1 [59,60]. Further, Equation (61e) ensures the shear strength ability of the weaker cross-section portions, Equation (61f) is a geometrical constraint ensuring that the cross-section of the weaker portion is fully connected with the one of the central portion (so guaranteeing that no undesired stress concentrations can occur) and Equation (61g) is a geometrical constraint describing the assumed beam scheme.

Equation (61h) ensures that the maximum beam deflection is not greater than the admissible assigned one f_{adm}. The expression of the relevant deflection has been obtained by solving the multistep continuum elastic analysis problem by means of a displacement method in Mathematica® 14.3 environment.

Equation (61i) ensures that the clamped cross-section (where the maximum bending moment acts) behaves elastically. This equation has been determined imposing that the bending moment at the clamped cross-section is given by the plastic one $W_{pym}\sigma_0$ acting in the section connecting the external M and the weak m portions, plus the contribution of the shear and that of the distributed loading in the M portion.

Equation (61j) represents the yield condition for the most stressed cross-section of the weaker portion; indeed, it imposes that the plastic resistance modulus of the relevant cross-section produces a limit bending moment equal to the suffered bending moment in limit collapse conditions.

Equation (61k) imposes that the central portion cross-section possesses bending strength not less than that of the weaker portions, so ensuring that no plastic strains can occur in correspondence with the connection between m and c portions.

Finally, Equation (61l) ensures that the cross-section of the central c portion behaves elastically under the maximum bending moment acting at the mid-span section.

It is worth noting that problem (61) can be regarded as a multicriteria optimal design; indeed, even if the objective function utilized is the minimum volume, the position (58) utilized for the length of the weaker portion of the multistep beam actually represents the optimal choice that ensures the occurrence of the maximum plastic dissipation. This remark is particularly relevant since the real goal of the design is the full exploitation of the structure capacity, always respecting the appropriate displacement and the strength safety criteria.

4. Applications and Results

This section is devoted to the solution of the optimal design problem (61) applied to the simple case of a perfectly clamped beam subjected to a uniformly distributed load. The chosen application allows a clear interpretation of the results for an appropriate judgment on the reliability of the approach, and it can be certainly regarded as representative of a typical beam belonging to a frame. The relevant data are reported in the following Figure 13.

As was stated in the previous section, the geometry of the rectangular cross-section (base b and height h) defining the contour of the stronger cross-section portion and the common web thickness of all the different cross-sections of the multistep beam must be assigned as data of the optimal design problem. On the other hand, as it is well known, the beams usually adopted in structural applications belong mainly to two different profiles (the HE and the IPE ones) which show quite different behavior.

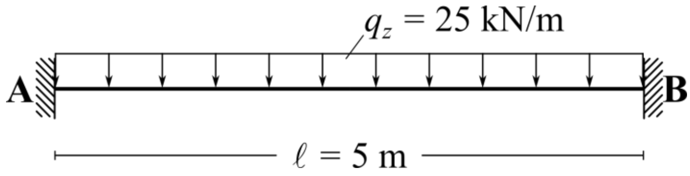

Figure 13. Perfectly clamped beam subjected to a uniformly distributed load.

Consequently, the first step has been the solution of a simple sub-optimal design in order to identify the beams on sale, whose cross-section belongs to HE and IPE profiles, satisfying the mechanical condition that the clamped section behaves elastically under the bending moment related to the ultimate condition and the kinematical condition that the beam deflection fulfills the standard requirement in serviceability conditions. The obtained beams are an HEA200 and an IPE270, whose geometrical characteristics together with the mechanical ones and the loading and kinematical conditions are reported in the following Table 3. It is worth noting that the obtained steel profiles satisfy the imposed constraints, but no plastic dissipation can be produced.

Table 3. Geometrical and mechanical characteristics of the beam to be optimally designed.

Description	HEA200 Beam	IPE270 Beam
Length ℓ	5.0 m	5.0 m
Base b	200 mm	135 mm
Height h	190 mm	270 mm
Web thickness t_w	6.5 mm	6.6 mm
Flange thickness t_f	10.0 mm	10.2 mm
Area A	53.83 cm^2	45.95 cm^2
E	210 GPa	
σ_0	235 MPa	
ξ_S	1.0	
ξ_L	1.5	
η_0	1.1	
q_z	25 kN/m	
f_{adm}	$\ell/300$	

For each selected profile, two different approaches have been adopted in performing the optimal design of the multistep beam: in the first one, the length ℓ_M of the beam portions close to the joint is regarded as free design variable, while in the second one $\ell_M = \ell_m$ has been imposed. By adopting such approaches, the influence of the length ℓ_M on the plastic dissipation will be evidenced. The optimal design problem has been solved in Mathematica® 14.3 environment by the FindMinimum command which adopts the interior point method to solve the optimization problem.

The results obtained by the solution of the optimal design problem (61), following the described approaches, are reported in Table 4 and in Table 5, respectively, for ℓ_M considered as free design variable and for $\ell_M = \ell_m$ in the case of HEA200 beam. The last row of the tables reports the amount of plastic dissipation calculated by means of Equation (53).

Table 4. Results for the multistep beam (HEA200 profile, ℓ_M free design variable).

Description	Value
Length ℓ_M	463.984 mm
Base b_M	200 mm
Height h_M	190 mm
Web thickness t_{wM}	6.5 mm
Flange thickness t_{fM}	14.378 mm
Length ℓ_m	125.745 mm
Base b_m	66.508 mm
Height h_m	187.381 mm
Web thickness t_{wm}	6.5 mm
Flange thickness t_{fm}	11.759 mm
Length ℓ_c	3820.542 mm
Base b_c	108.658 mm
Height h_c	183.906 mm
Web thickness t_{wc}	6.5 mm
Flange thickness t_{fc}	8.284 mm
V	0.0180 m^3
Volume saving	33.12%
D_p	22,452 Nmm

Table 5. Results for the multistep beam (HEA200 profile, $\ell_M = \ell_m$.

Description	Value
Length ℓ_M	92.668 mm
Base b_M	200 mm
Height h_M	190 mm
Web thickness t_{wM}	6.5 mm
Flange thickness t_{fM}	11.635 mm
Length ℓ_m	92.668 mm
Base b_m	135.215 mm
Height h_m	190 mm
Web thickness t_{wm}	6.5 mm
Flange thickness t_{fm}	11.635 mm
Length ℓ_c	4629.328 mm
Base b_c	176.486 mm
Height h_c	187.086 mm
Web thickness t_{wc}	6.5 mm
Flange thickness t_{fc}	8.721 mm
V	0.0212 m^3
Volume saving	21.23%
D_p	35,192 Nmm

In Tables 6 and 7 the analogous results are reported, always obtained by the two different approaches, for the case of IPE270 beam. The last row of the tables reports the amount of plastic dissipation calculated by means of Equation (53).

Table 6. Results for the multistep beam (IPE270 profile, ℓ_M free design variable).

Description	Value
Length ℓ_M	453.862 mm
Base b_M	135 mm
Height h_M	270 mm
Web thickness t_{wM}	6.6 mm
Flange thickness t_{fM}	12.084 mm
Length ℓ_m	196.310 mm
Base b_m	33.080 mm
Height h_m	267.640 mm
Web thickness t_{wm}	6.6 mm
Flange thickness t_{fm}	9.724 mm
Length ℓ_c	3699.656 mm
Base b_c	46.661 mm
Height h_c	267.445 mm
Web thickness t_{wc}	6.6 mm
Flange thickness t_{fc}	9.529 mm
V	0.0147 m^3
Volume saving	36.02%
D_p	27,451 Nmm

Table 7. Results for the multistep beam (IPE270 profile, $\ell_M = \ell_m$.

Description	Value
Length ℓ_M	131.966 mm
Base b_M	135 mm
Height h_M	270 mm
Web thickness t_{wM}	6.6 mm
Flange thickness t_{fM}	16.832 mm
Length ℓ_m	131.966 mm
Base b_m	67.846 mm
Height h_m	265.609 mm
Web thickness t_{wm}	6.6 mm
Flange thickness t_{fm}	12.441 mm
Length ℓ_c	4472.136 mm
Base b_c	104.205 mm
Height h_c	266.763 mm
Web thickness t_{wc}	6.6 mm
Flange thickness t_{fc}	13.595 mm
V	0.0222 m^3
Volume saving	3.37%
D_p	31,850 Nmm

Furthermore, in Figure 14a,b and in Figure 14c,d the obtained optimal beams for the case of HEA200 are sketched for ℓ_M free design variable and for $\ell_M = \ell_m$.

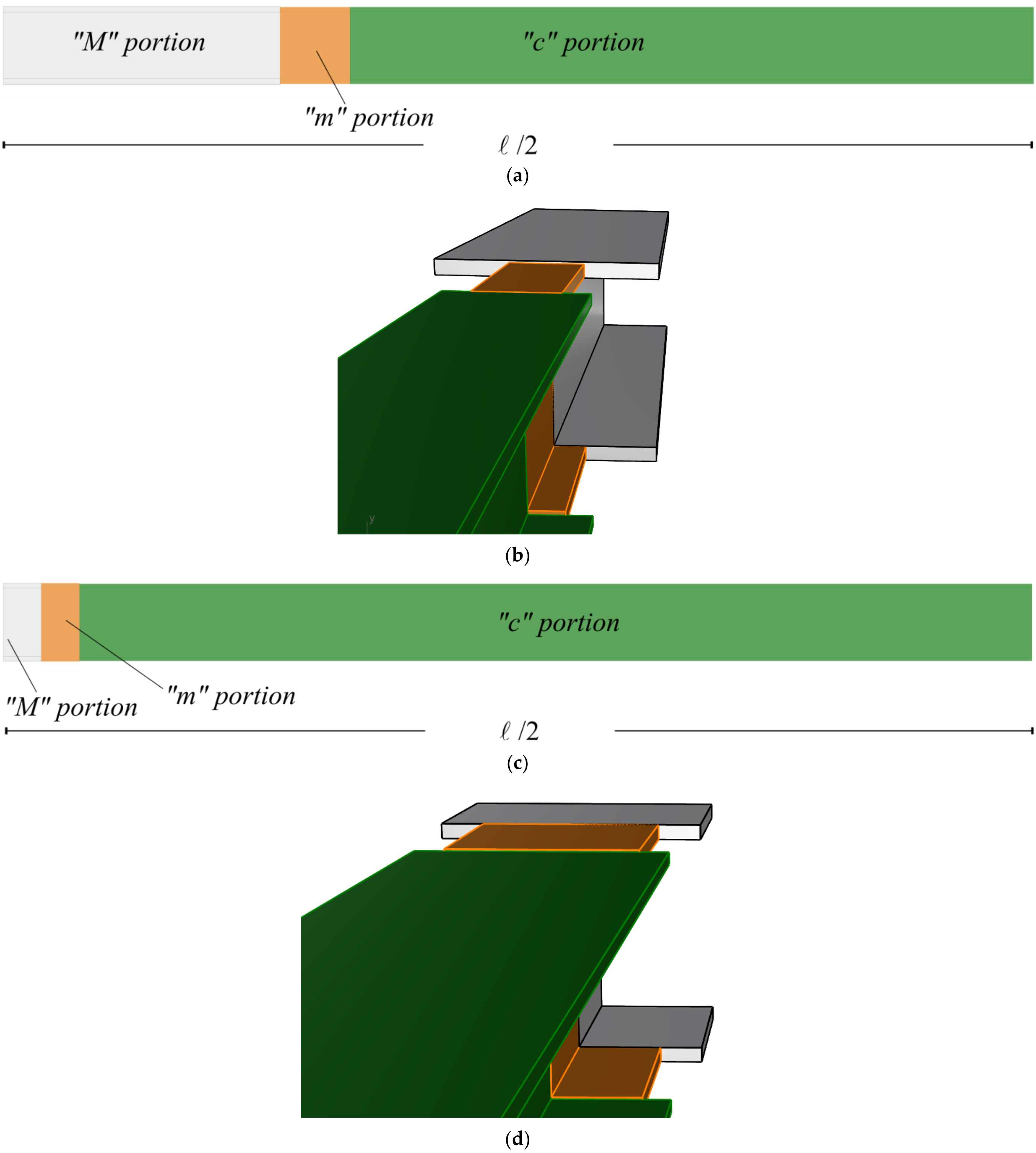

Figure 14. Optimal beam for HEA200 profile: (**a**) ℓ_M free design variable lateral view; (**b**) ℓ_M free design variable particular of the perspective view; (**c**) $\ell_M = \ell_m$ lateral view; (**d**) $\ell_M = \ell_m$ particular of the perspective view.

Finally, in Figure 15a,b and in Figure 15c,d the obtained optimal beams for the case of IPE270 are sketched for ℓ_M free design variable and for $\ell_M = \ell_m$.

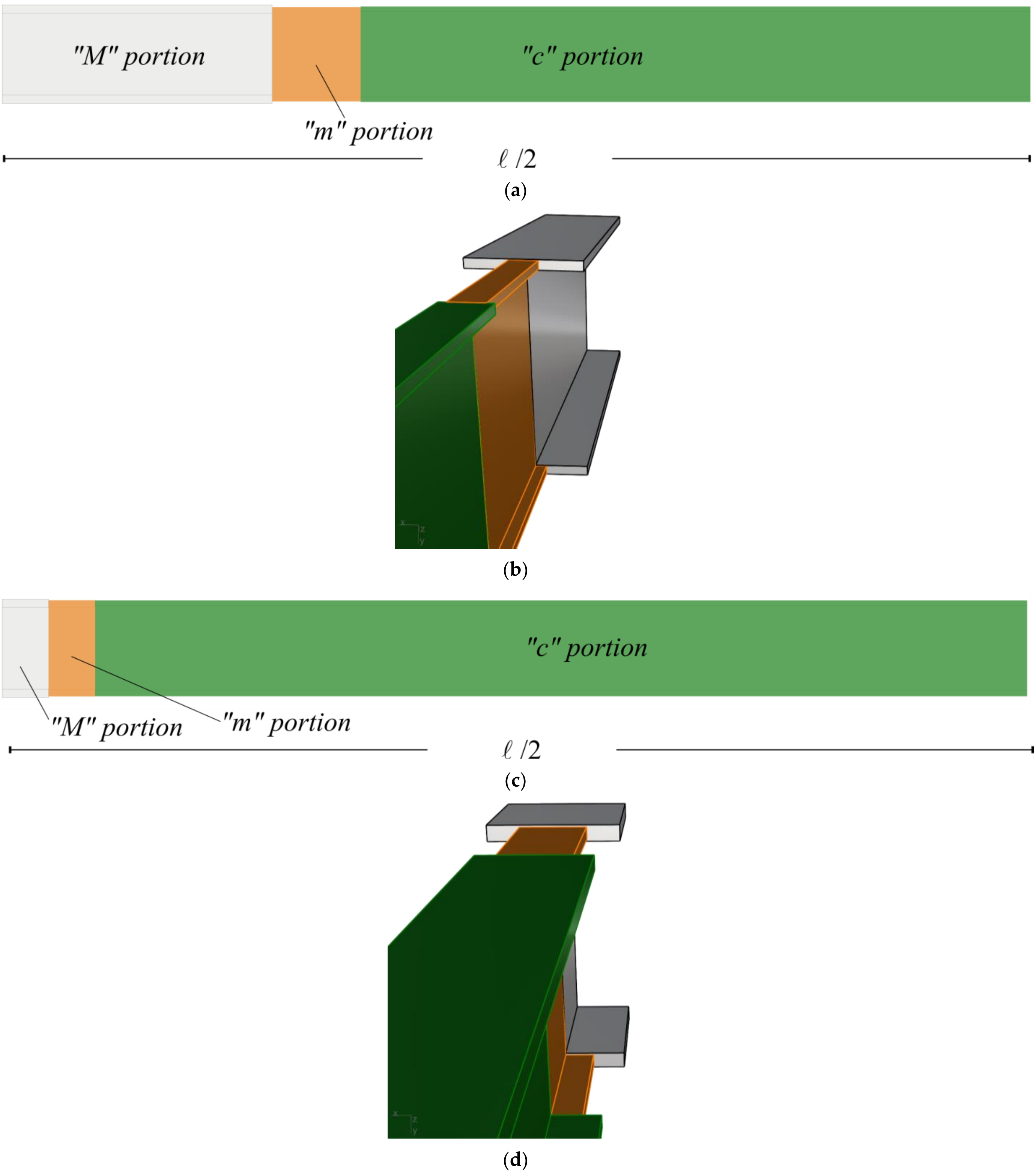

Figure 15. Optimal beam for IPE240 profile: (**a**) ℓ_M free design variable lateral view; (**b**) ℓ_M free design variable particular of the perspective view; (**c**) $\ell_M = \ell_m$ lateral view; (**d**) $\ell_M = \ell_m$ particular of the perspective view.

An examination of the obtained results allows us to state that all the obtained designs are characterized by a significant volume saving and a considerable amount of plastic dissipation produced. However, it is worth noting that the two different approaches show different trends. Indeed, in the case in which ℓ_M is a free design variable, the weaker portion tends to go away from the beam–column connection (i.e., ℓ_M tends to increase) so reducing its cross-section dimensions and increasing ℓ_m related to a portion of bending moment distribution characterized by slight slope. These features implicate that the notable volume saving is related to a modest plastic dissipation produced. On the other hand, in the case in which $\ell_M = \ell_m$ is imposed, the weaker portion rests close to the clamped cross-section involving a portion of bending moment distribution characterized by high slope. These features implicate that volume saving is not so great, but it is related to a great plastic dissipation produced, and this result is essential for a real good behavior of the designed beam. Since the main goal of the proposed approach is to determine a beam able to perform as much plastic dissipation as possible, this last remark suggests that the case in which $\ell_M = \ell_m$ is the most favorable one with the further suggestion to select ℓ_M as short as possible depending on technological requirements. In other words, ℓ_M must be short enough to ensure the desired great amount of plastic dissipation and long enough to ensure that the stress distribution in correspondence of the end cross-sections remains below the yield limit.

To verify the last remark, the mechanical behavior of optimal beams reported in Tables 5 and 7 has been checked by suitable modeling in ABAQUS® 2017 environment. The optimal beams have been meshed by adopting 3D C3D8R solid element type, assuming the elastic–perfectly plastic behavior of steel S235 as reported in Table 3. The obtained number of elements is 184,434 (corresponding to 297,888 nodes) for the optimal beam in Table 5 and 206,182 (corresponding to 297,492 nodes) for the one in Table 7. The results, in terms of Mises stress, corresponding to maximum allowable load, are reported in Figure 16.

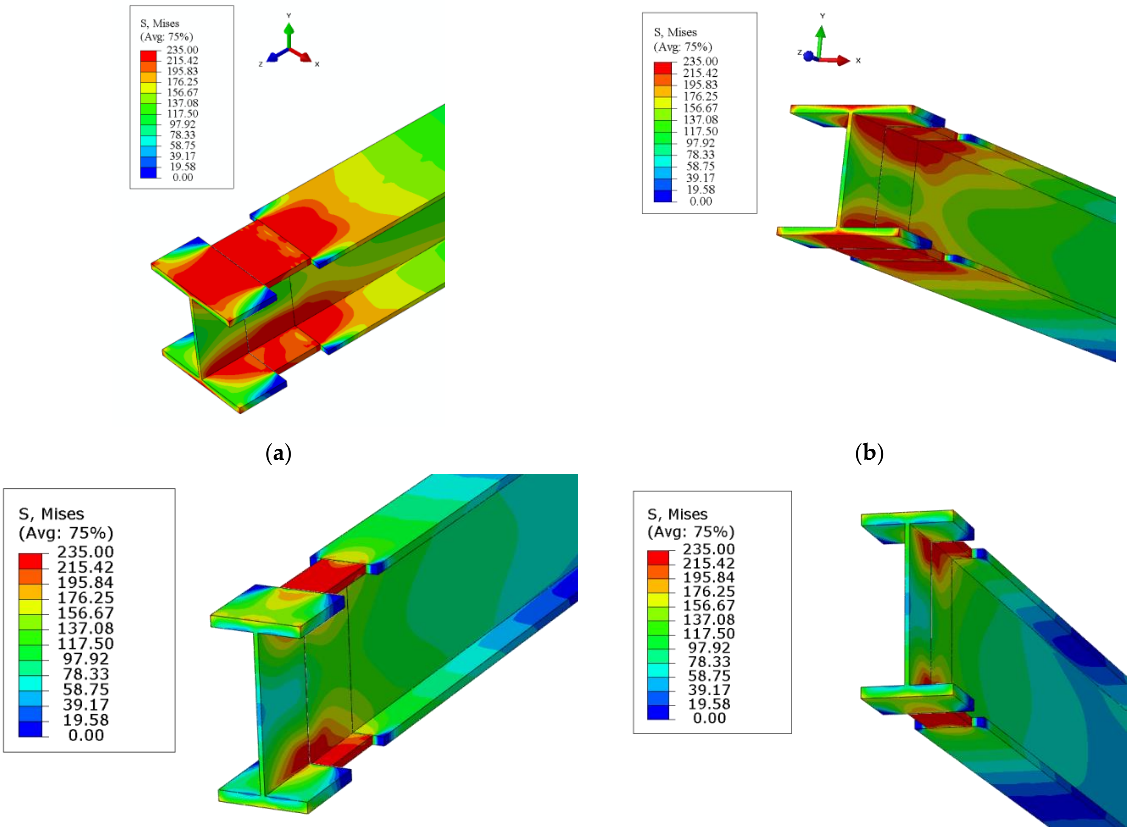

Figure 16. Maps of Mises stress in the weak portion of the optimal beams: (**a**,**b**) Case of HEA 200 cross-section (Table 5); (**c**,**d**) Case of IPE 240 cross-section (Table 7).

An examination of these figures confirms the affordability of the proposed optimal design, since—as it can be easily observed—the weak portion of the optimal beams can be regarded as almost fully plasticized while the other portions still behave elastically (IPE270) or show very small plasticized zones. The maximum deflection obtained by the FEM models is equal to 14.63 mm for the beam in Table 5 and 9.668 mm for the beam in Table 7, respectively. Both values are admissible since the standard limit is equal to 16.67 mm.

Finally, it is worth noting that the reliability of the proposed formulation does not depend on the load intensity variation and/or on the beam length; indeed, in the optimal design problem (61) the design variables are continuous ones, so ensuring a real optimal solution for any variation in the load intensity, while, in the case of the use of standard profiles, the discrete variation in the size cannot ensure an optimum design; furthermore, referring to the beam length, it can be stated that its increment produces an appropriate increment of the plastic dissipation in the optimal multistep beam due to the relation between the beam length and the weaker portion length, while, in any case, if the standard profile sub optimal beam is designed no plastic dissipation can be produced.

5. Conclusions

The present paper is mainly devoted to proposing the formulation of a special new version of the optimal minimum volume design of multistep steel beams able to maximize the exploitation of the material ductility, also preventing the brittle failure in correspondence of the welded connections. Clearly, the proposed optimal design will simultaneously fulfil all the usual safety requirements required by the structural standards both in serviceability condition and in ultimate limit load condition.

To guarantee the full exploitation of the beam ductility features, simultaneously minimizing the overall structural volume, the design problem has been formulated as a minimum volume one but imposing, by suitable constraints, that a selected portion of the beam, of appropriate length, is devoted to the onset of plastic deformations in ultimate state condition. This appropriate length has been rigorously defined by a prior study of the function describing the plastic deformation spread (in particular, the plastic curvature) in a bending steel beam.

The proposed formulation has been applied to the simple case of a perfectly clamped beam; however, such a simple example has been considered fully acceptable in order to prove the full reliability of the proposed approach and, furthermore, it can be regarded as certainly adequate to represent the main behavioral features related to beams belonging to steel frames.

The results obtained are extremely encouraging and have been confirmed by suitable 3D FEM analyses performed in ABAQUS® environment. They suggest clear information on the most appropriate constraints to impose on the optimal design problem. Specifically, it is clearly indicated that to guarantee the largest (optimal) plastic dissipation, the length of the external portions of the beam must be as small as possible respecting the technological requirements for welded sections. The proposed applications suggest this length to be equal to that of the weaker portions devoted to the onset of plastic deformations. Furthermore, the results obtained clearly suggest that for a better multistep beam design it is preferable to refer to the HE profile type rather than to the IPE one.

The results obtained will be further developed in the next papers which will be devoted to the extension of the proposed approach to plane steel frames as well as to three-dimensional ones considering, as indicated in structural standards, also wider loading combinations. Furthermore, experimental laboratory tests will also be carried out, devoted firstly to checking the technological aspects related to the factory production of the multistep beams, and successively the real behavior of frames constituted by multistep beam elements subjected to quasi static and dynamic loads.

Author Contributions: All authors equally contributed to the preparation of paper. All authors have read and agreed to the published version of the manuscript.

Funding: This research received no external funding.

Informed Consent Statement: Not applicable.

Data Availability Statement: Data are contained within the article.

Conflicts of Interest: The authors declare no conflicts of interest.

References

1. Gokhfeld, D.A.; Cherniavsky, D.F. *Limit Analysis of Structures at Thermal Cycling*; Springer: Dordrecht, The Netherland, 1980; ISBN 978-90-286-0455-1.
2. Marti, K. Limit load and shakedown analysis of plastic structures under stochastic uncertainty. *Comput. Meth. App. Mech. Eng.* **2008**, *198*, 42–51. [CrossRef]
3. Heitzer, M.; Staat, M. Reliability analysis of elastoplastic structures under variable loads. In *Inelastic Analysis of Structures Under Variable Loads*; Weichert, D., Maier, G., Eds.; Volume 83 of Solid mechanics and its applications; Springer: Berlin, Germany, 2000; pp. 269–288.
4. Chen, W.; Duan, L. *Plasticity, Limit Analysis, Stability and Structural Design: An Academic Life Journey from Theory to Practice*; World Scientific: Singapore, 2021; ISBN 978-981122974-9, 978-981122973-2.
5. Asgarian, B.; Ordoubadi, B. Effects of structural uncertainties on seismic performance of steel moment resisting frames. *J. Constr. Steel Res.* **2016**, *120*, 132–142. [CrossRef]
6. Ghasemof, A.; Mirtaheri, M.; Mohammadi, R.K.; Salkhordeh, M. A multi-objective optimization framework for optimally designing steel moment frame structures under multiple seismic excitations. *Earthq. Struct.* **2022**, *23*, 35–57. [CrossRef]
7. Zhang, R.; Wang, W.; Alam, M.S. Seismic evaluation of friction spring-based self-centering braced frames based on life-cycle cost. *Earthq. Eng. Struct. Dyn.* **2022**, *51*, 3393–3415. [CrossRef]
8. Hu, S.; Zhu, S. Life-cycle benefits estimation for hybrid seismic-resistant self-centering braced frames. *Earthq. Eng. Struct. Dyn.* **2023**, *52*, 3097–3119. [CrossRef]
9. Banichuk, N.V. *Introduction to Optimization of Structures*; Springer: New York, NY, USA, 1990; ISBN 978-1-4612-7988-4. [CrossRef]
10. Huang, M.F.; Li, Q.; Chan, C.M.; Lou, W.J.; Kwok, K.C.S.; Li, G. Performance-based design optimization of tall concrete framed structures subject to wind excitations. *J. Wind Eng. Ind. Aerodyn.* **2015**, *139*, 70–81. [CrossRef]
11. Se-Hyu, C.; Seung-Eock, K. Optimal design of steel frame using practical nonlinear inelastic analysis. *Eng. Struct.* **2002**, *24*, 1189–1201. [CrossRef]
12. Degertekin, S.O. Improved harmony search algorithms for sizing optimization of truss structures. *Comput. Struct.* **2012**, *92–93*, 229–241. [CrossRef]
13. Kaveh, H.; Nasrollahi, A. Performed-based seismic design of steel frames utilizing charged system search optimization. *Appl. Soft Comput.* **2014**, *22*, 213–221. [CrossRef]
14. Atkočiūnas, J.; Liepa, L.; Blaževičius, G.; Merkevičiūtė, D. Solution validation technique for optimal shakedown design problems. *Struct. Multidisc. Optim.* **2017**, *56*, 853–863. [CrossRef]
15. Palizzolo, L.; Benfratello, S.; Tabbuso, P. Discrete variable design of frames subjected to seismic actions accounting for element slenderness. *Comput. Struct.* **2015**, *147*, 147–158. [CrossRef]
16. Tunca, O.; Carbas, S. Sustainable and cost-efficient design optimization of rectangular and circular-sectioned reinforced concrete columns considering slenderness and eccentricity. *Structures* **2024**, *61*, 105989. [CrossRef]
17. Zhang, R.; Hu, S. Optimal design of self-centering braced frames with limited self-centering braces. *J. Build. Eng.* **2024**, *88*, 109201. [CrossRef]
18. Miller, D.K. Lessons learned from the Northridge earthquake. *Eng. Struct.* **1998**, *20*, 249–260. [CrossRef]
19. Mahin, S.T. Lessons from damage to steel buildings during the Northridge earthquake. *Eng. Struct.* **1998**, *20*, 261–270. [CrossRef]
20. Wang, M.; Shi, Y.; Wang, Y.; Shi, G. Numerical study on seismic behaviors of steel frame end-plate connections. *J. Constr. Steel Res.* **2013**, *90*, 140–152. [CrossRef]
21. Xu, Q.; Chen, H.; Li, W.; Zheng, S.; Zhang, X. Experimental investigation on seismic behavior of steel welded connections considering the influence of structural forms. *Eng. Fail. Anal.* **2022**, *139*, 106499. [CrossRef]
22. Iwankiw, N.R.; Carter, C.J. The dogbone: A new idea to chew on. *Mod. Steel Constr.* **1996**, *36*, 18–23.
23. Plumier, A. The dogbone: Back to the future. *Eng. J.* **1997**, *34*, 61–67. [CrossRef]

24. Morshedi, M.A.; Dolatshahi, K.M.; Maleki, S. Double reduced beam section connection. *J. Constr. Steel Res.* **2017**, *138*, 283–297. [CrossRef]
25. Sofias, C.E.; Pachoumis, D.T. Assessment of reduced beam section (RBS) moment connections subjected to cyclic loading. *J. Constr. Steel Res.* **2020**, *171*, 106151. [CrossRef]
26. Engelhardt, M.D.; Winneberger, T.; Zekany, A.J.; Potyray, T.J. Experimental investigation of dogbone moment connections. *Eng. J.* **1998**, *35*, 128–139. [CrossRef]
27. Saleh, A.; Mirghaderi, S.R.; Zahrai, S.M. Cyclic testing of tubular web RBS connections in deep beams. *J. Constr. Steel Res.* **2016**, *117*, 214–226. [CrossRef]
28. Mirghaderi, S.R.; Shahabeddin, T.; Imanpour, A. Seismic performance of the accordion-web RBS connection. *J. Constr. Steel Res.* **2010**, *66*, 277–288. [CrossRef]
29. Momenzadeh, S.; Kazemi, M.T.; Asl, M.H. Seismic performance of reduced web section moment connections. *Int. J. Steel Struct.* **2017**, *17*, 413–425. [CrossRef]
30. Horton, T.A.; Hajirasouliha, I.; Davison, B.; Ozdemir, Z. More efficient design of reduced beam sections (RBS) for maximum seismic performance. *J. Constr. Steel Res.* **2021**, *183*, 106728. [CrossRef]
31. Gerami, M.; Bahirai, M. Seismic Rehabilitation of Steel Frame Connections Through Asymmetrically Weakening the Beam. *Int. J. Steel Struct.* **2019**, *19*, 1209–1224. [CrossRef]
32. Feng, S.; Yang, Y.; Hao, N.; Chen, X.; Zhou, J. Experimental Study on Hysteretic Performance of Steel Moment Connection with Buckling-Restrained Dog-Bone Beam Sections. *Buildings* **2024**, *14*, 760. [CrossRef]
33. Tabar, A.M.; Alonso-Rodriguez, A.; Tsavdaridis, K.D. Building retrofit with reduced web (RWS) and beam (RBS) section limited-ductility connections. *J. Constr. Steel Res.* **2022**, *197*, 107459. [CrossRef]
34. Vayas, I.; Karydakis, P.; Dimakogianni, D.; Dougka, G. *Dissipative Devices for Seismic Resistant Steel Frames—The FUSEIS Project*; Final Report; Research Programme of the Research Fund for Coal and Steel; Publications Office of the EU: Luxembourg, 2012.
35. Calado, L.; Proenca, J.M.; Espinha, M.; Castiglioni, C.A. Hysteretic behaviour of dissipative bolted fuses for earthquake re-sistant steel frames. *J. Constr. Steel Res.* **2013**, *85*, 151–162. [CrossRef]
36. Calado, L.; Proenca, J.M.; Espinha, M.; Castiglioni, C.A. Hysteretic behavior of dissipative welded fuses for earthquake re-sistant composite steel and concrete frames. *Steel Comp. Struct.* **2013**, *14*, 547–569. [CrossRef]
37. Dougka, G.; Dimakogianni, D.; Vayas, I. Seismic behavior of frames with innovative energy dissipation systems (FUSEIS 1-1). *Earthq. Struct.* **2014**, *6*, 561–580. [CrossRef]
38. Kanyilmaz, A.; Muhaxheri, M.; Castiglioni, C.A. Influence of repairable bolted dissipative beam splices (structural fuses) on reducing the seismic vulnerability of steel-concrete composite frames. *Soil Dyn. Earthq. Eng.* **2019**, *119*, 281–298. [CrossRef]
39. Tsarpalis, P.; Bakalis, K.; Thanopoulos, P.; Vayas, I.; Vamvatsikos, D. Pre-normative assessment of behaviour factor for lateral load resisting system FUSEIS pin-link. *Bull. Earthq. Eng.* **2020**, *18*, 2681–2698. [CrossRef]
40. Avgerinou, S.; Thanopoulos, P.; Hoffmeister, B.; Vayas, I. Seismic resistant buildings with dissipative elements made of high strength steel [Erdbebensichere Bauten mit dissipativen Elementen aus hochfestem Stahl]. *Stahlbau* **2022**, *91*, 326–337. [CrossRef]
41. Valente, M.; Castiglioni, C.A.; Kanyilmaz, A. Numerical investigations of repairable dissipative bolted fuses for earthquake resistant composite steel frames. *Eng. Struct.* **2017**, *131*, 275–292. [CrossRef]
42. Valente, M.; Castiglioni, C.A.; Kanyilmaz, A. Welded fuses for dissipative beam-to-column connections of composite steel frames: Numerical analyses. *J. Constr. Steel Res.* **2017**, *128*, 498–511. [CrossRef]
43. Calado, L.; Proença, J.M.; Sio, J.F.A. Composite Frames with Dissipative Beam Splices: Numerical Analyses and Design Guidelines. *Key Eng. Mat.* **2018**, *763*, 771–778. [CrossRef]
44. Tahamouli Roudsari, M.; Jamshidi, K.H.; Akbari, G.F.; Torkaman, M. An experimental and numerical investigation of reduced beam section connections with horizontal and vertical web stiffeners. *Asian J. Civ. Eng.* **2020**, *21*, 581–595. [CrossRef]
45. Castiglioni, C.A.; Kanyilmaz, A.; Calado, L. Experimental analysis of seismic resistant composite steel frames with dissipative devices. *J. Constr. Steel Res.* **2012**, *76*, 1–12. [CrossRef]
46. Dougka, G.; Dimakogianni, D.; Vayas, I. Innovative energy dissipation systems (FUSEIS 1-1)—Experimental analysis. *J. Constr. Steel Res.* **2014**, *96*, 69–80. [CrossRef]
47. Avgerinou, S.; Vayas, I. High-strength steel on dissipative elements in seismic resistant systems: Tests and simulations. *J. Constr. Steel Res.* **2020**, *172*, 106173. [CrossRef]
48. Benfratello, S.; Palizzolo, L. Limited resistance rigid perfectly plastic hinges for steel frames. *Intern. Rev. Civ. Eng.* **2017**, *8*, 286–298. [CrossRef]
49. Benfratello, S.; Palizzolo, L.; Tabbuso, P.; Vazzano, S. On the post elastic behavior of LRPH connections. *Int. Rev. Model. Simul.* **2019**, *12*, 341–353. [CrossRef]
50. Benfratello, S.; Palizzolo, L.; Tabbuso, P.; Vazzano, S. LRPH device optimization for axial and shear stresses. *Intern. Rev. Civ. Eng.* **2020**, *11*, 152–163. [CrossRef]

51. Palizzolo, L.; Benfratello, S.; Tabbuso, P.; Vazzano, S. Numerical validation of LRPH behaviour by fem analysis. In *Advances in Engineering Materials, Structures and Systems: Innovations, Mechanics and Applications—Proceedings of the 7th International Conference on Structural Engineering, Mechanics and Computation, Cape Town, South Africa, 2–4 September 2019*; CRC Press/Balkema: Leiden, The Netherlands, 2019; pp. 1224–1229. [CrossRef]
52. Benfratello, S.; Palizzolo, L.; Vazzano, S. Experimental analysis of new moment resisting steel connections. In Proceedings of the 25th Conference of the Italian Association of Theoretical and Applied Mechanics, AIMETA 2022, Palermo, Italy, 4–8 September 2022. [CrossRef]
53. Benfratello, S.; Palizzolo, L. Prevention of brittle failure for steel connections utilizing special devices. *Structures* **2024**, *62*, 106153. [CrossRef]
54. Benfratello, S.; Palizzolo, L.; Vazzano, S. A New Design Problem in the Formulation of a Special Moment Resisting Connection Device for Preventing Local Buckling. *J. Appl. Sci.* **2022**, *12*, 202. [CrossRef]
55. Benfratello, S.; Caddemi, S.; Palizzolo, L.; Pantò, B.; Rapicavoli, D.; Vazzano, S. Targeted steel frames by means of innovative moment resisting connections. *J. Constr. Steel Res.* **2021**, *183*, 106695. [CrossRef]
56. Pantò, B.; Rapicavoli, D.; Caddemi, S.; Caliò, I. A smart displacement based (SDB) beam element with distributed plasticity. *Appl. Math. Model.* **2017**, *44*, 336–356. [CrossRef]
57. Pantò, B.; Rapicavoli, D.; Caddemi, S.; Caliò, I. A fibre smart displacement based (FSDB) beam element for the nonlinear analysis of reinforced concrete members. *Intern. J. Non-Linear Mech.* **2019**, *117*, 103222. [CrossRef]
58. Benfratello, S.; Caddemi, S.; Palizzolo, L.; Pantò, B.; Rapicavoli, D. A New Iterative Design Strategy for Steel Frames Modelled by Generalised Multi-stepped Beam Elements. *Buildings* **2024**, *14*, 2155. [CrossRef]
59. *EN 1998-3:2005*; Eurocode 8: Design of Structures for Earthquake Resistance—Part 3: Assessment and Retrofitting of Buildings. Comité Européen de Normalisation: Brussels, Belgium, 2005.
60. *EN 1993-1-8:2006*; Eurocode 3: Design of Steel Structures Part 1–8: Design of Joints. European Committee for Standardization: Brussels, Belgium, 2006.